Two-photon imaging of remyelination of spinal cord axons by engrafted neural precursor cells in a viral model of multiple sclerosis

Milton L. Greenberg[a,b,1], Jason G. Weinger[c,d,1], Melanie P. Matheu[a,b,2], Kevin S. Carbajal[c,d,3], Ian Parker[a,e], Wendy B. Macklin[f], Thomas E. Lane[b,c,d,g,4,5], and Michael D. Cahalan[a,b,g,5]

[a]Department of Physiology and Biophysics, [b]Institute for Immunology, [c]Department of Molecular Biology and Biochemistry, [d]Sue and Bill Gross Stem Cell Center, [e]Department of Neurobiology and Behavior, and [g]Multiple Sclerosis Research Center, University of California, Irvine, CA 92697; and [f]Department of Cell and Developmental Biology, University of Colorado School of Medicine, Aurora, CO 80045

Contributed by Michael D. Cahalan, April 18, 2014 (sent for review February 18, 2014)

Neural precursor cells (NPCs) offer a promising approach for treating demyelinating diseases. However, the cellular dynamics that underlie transplanted NPC-mediated remyelination have not been described. Using two-photon imaging of a newly developed ventral spinal cord preparation and a viral model of demyelination, we describe the motility and intercellular interactions of transplanted mouse NPCs expressing green fluorescent protein (GFP) with damaged axons expressing yellow fluorescent protein (YFP). Our findings reveal focal axonal degeneration that occurs in the ventral side of the spinal cord within 1 wk following intracranial instillation with the neurotropic JHM strain of mouse hepatitis virus (JHMV). Axonal damage precedes extensive demyelination and is characterized by swelling along the length of the axon, loss of YFP signal, and transected appearance. NPCs engrafted into spinal cords of JHMV-infected mice exhibited diminished migration velocities and increased proliferation compared with transplanted cells in noninfected mice. NPCs preferentially accumulated within areas of axonal damage, initiated direct contact with axons, and subsequently expressed the myelin proteolipid protein gene, initiating remyelination. These findings indicate that NPCs transplanted into an inflammatory demyelinating microenvironment participate directly in therapeutic outcome through the wrapping of myelin around damaged neurons.

stem | microscopy | differentiation | myelination | central nervous system

Multiple sclerosis (MS) is a chronic inflammatory disease of the central nervous system (CNS) that results in demyelination and axonal loss, culminating in extensive disability through defects in neurologic function (1). The demyelination that defines MS pathology is progressive over time; however, spontaneous yet transient myelin repair can occur during the course of disease (2). Currently approved therapies for treating MS are designed to limit immune cell infiltration into the CNS to mute demyelination and impede the emergence of new lesions (3). Recent studies from our laboratory and others have shown that engraftment of neural precursor cells (NPCs) may provide an important unmet clinical need for MS patients by facilitating sustained remyelination that can restore motor function and ameliorate clinical symptoms associated with demyelinating disease. NPC engraftment is well tolerated in animal models and contributes to clinical recovery associated with remyelination, highlighting the feasibility of using NPCs for treating demyelinating diseases (4–8). Indeed, transplantation of human NPCs into the frontal lobes of children with Pelizaeus–Merzbacher disease (PMD), a rare genetic disorder that affects the growth of the myelin sheath, has revealed measurable gains in motor and/or cognition skills, emphasizing the translational relevance of NPCs for treatment of white matter diseases (9).

Although NPCs have been shown to migrate and facilitate remyelination in preclinical animal models of demyelination, the motility characteristics and interactions of NPCs with damaged axons have not directly been visualized in real time within the intact cord. Instead, imaging has been limited to "snapshots" of NPCs transplanted into the spinal cord and visualized in fixed tissue by immunohistochemistry or with fluorescently labeled engrafted cells (8, 10, 11). In this study, we used a mouse model of viral-induced demyelination to establish an alternative imaging system enabling stable ex vivo imaging of transplanted GFP-labeled mouse NPCs within the ventral murine spinal cord through use of two-photon (2P) microscopy. Mice persistently infected with the neurotropic JHM strain of mouse hepatitis virus (JHMV) develop MS-like symptoms ranging from partial to complete hind limb paralysis that are associated with immune cell accumulation within the CNS and white matter damage (12–16). We have previously demonstrated that engraftment of syngeneic mouse NPCs promotes clinical recovery that correlates with increased axonal integrity and remyelination (8), although neuroinflammation is not affected (17). Transplanted NPCs follow a CXCL12 chemokine gradient to preferentially colonize areas of white matter damage, where a majority of cells differentiate into an oligodendrocyte lineage (5, 8).

Two-photon microscopy enables real-time visualization of cellular migration and intercellular interactions within intact organs (18). Several groups have used 2P microscopy to characterize axonal degradation and immune cell dynamics in the

Significance

Stem cell transplantation has emerged as a promising cell-based therapy for the treatment of demyelinating diseases such as multiple sclerosis (MS). This study provides the first real-time imaging of transplanted stem cell-mediated remyelination in a mouse model of MS. Whereas current treatments solely delay disease progression, transplanted stem cells actively reverse clinical disease in animal models. Using two-photon microscopy and viral-induced demyelination, we describe a technique to visualize cellular migration and remyelination in the mouse spinal cord. Transplanted neural precursor cells physically wrap damaged axons with newly formed myelin, preserving axonal health.

Author contributions: M.L.G., J.G.W., M.P.M., W.B.M., T.E.L., and M.D.C. designed research; M.L.G., J.G.W., M.P.M., and K.S.C. performed research; W.B.M. contributed new reagents/analytic tools; M.L.G. and J.G.W. analyzed data; and M.L.G., J.G.W., I.P., T.E.L., and M.D.C. wrote the paper.

The authors declare no conflict of interest.

[1]M.L.G. and J.G.W. contributed equally to this work.

[2]Present address: Diabetes Center, University of California, San Francisco, CA 94143.

[3]Present address: Department of Neurology, University of Michigan School of Medicine, Ann Arbor, MI 48109.

[4]Present address: Division of Microbiology and Immunology, Department of Pathology, University of Utah School of Medicine, Salt Lake City, UT 84132.

[5]To whom correspondence may be addressed. E-mail: mcahalan@uci.edu or tom.lane@path.utah.edu.

This article contains supporting information online at www.pnas.org/lookup/suppl/doi:10.1073/pnas.1406658111/-/DCSupplemental.

dorsal spinal cord during demyelinating disease progression (19–23). However, because engrafted NPCs preferentially migrate to regions deep within the ventral spinal cord (24), standard dorsal-side 2P in vivo imaging techniques are not suitable for visualization deep in the ventral side. Using a ventral-side imaging preparation, we now demonstrate that NPCs transplanted into the spinal cords of JHMV-infected mice under pathologic conditions migrate directionally, take up residence in regions of axonal degradation, colocalize with damaged axons, and facilitate remyelination through direct interactions with axons.

Results

Live-Cell Imaging of Axonal Degeneration in the Ventral Spinal Cord. To establish a system for ex vivo imaging in the ventral side of the murine spinal cord, we isolated the spinal cord from thoracic vertebra 4 to lumbar vertebra 2. The explanted spinal cord was embedded in a 5% agarose gel to maintain spinal cord integrity during superfusion with oxygenated medium (Fig. 1*A*) and was subsequently imaged by 2P microscopy. We used transgenic Thy1-YFP mice, which express yellow fluorescent protein (YFP) in a subset of medium- to large-caliber axons (25, 26), to study axonal pathology in the ventral spinal cord during the course of demyelination following JHMV infection. Lesions in the ventral spinal cord contained axons displaying a spectrum of "focal axonal degeneration" (FAD) [an established scale of axonal damage (20)] morphologies (Fig. 1*B*). Long, continuous axons with no damage are defined as "FAD stage 0"; FAD stage 1 axons contain focal swellings progressing along the length of the axon; and FAD stage 2 axons have gaps separating areas of YFP fluorescence. Analysis of FAD at various time points following JHMV infection revealed a progression of axonal pathology (Fig. 1*C*), similar to studies examining FAD in the dorsal spinal cord following myelin oligodendrocyte glycoprotein (MOG) immunization (20). Whereas damaged axons were not observed in the noninfected mouse (Fig. 1*D*), rapid FAD progression was readily observed 7 d following JHMV infection, confirming that FAD was a result of JHMV infection (Fig. 1*E* and Movie S1).

Whereas FAD has been shown to be associated with mitochondrial and myelin damage (20), it is unknown whether FAD stage 2 axons are completely transected. To determine the extent of axonal transection in axons that had lost YFP signal, JHMV-infected spinal cord sections were examined for axonal damage by immunofluorescence microscopy of αSMI-32 staining, which detects a nonphosphorylated epitope in neurofilament H (27). In areas where the axonal YFP signal was markedly diminished and fractured, SMI-32 staining appeared punctate or absent, indicating severely damaged axons (Fig. 2*A*). We observed various stages of axonal damage along the length of a single axon (Fig. 2*B*), including areas of intact YFP signal without SMI-32 (intact healthy axon), YFP signal concomitant with SMI-32 (intact but damaged axon), no YFP or SMI-32 signal (transected area of axon without continuous neurofilament), and SMI-32 without YFP signal (intact but damaged axon). The latter case indicates that although a loss of YFP fluorescence correlates with varying degrees of axonal damage, it does not necessarily indicate complete axonal transection. We conclude that loss of YFP signal correlates with varying degrees of axonal damage, but not necessarily an irreversibly transected axon. Whereas both FAD 1 and FAD 2 axons had areas with axonal damage, axons exhibiting loss of both YFP and SMI32 at multiple loci were more common in FAD 2 axons (Fig. 2*C*). To verify that axonal regions devoid of both YFP and SMI-32 signal are completely transected, we performed immunohistochemical staining for SMI-31, an accepted marker for undamaged axonal regions (phosphorylated neurofilament H) (28). We were unable to detect SMI-31 without YFP signal along YFP-expressing axons (Fig. 2*D*). These findings support the conclusion that $YFP^{-}SMI\text{-}32^{-}$ axonal regions are transected.

Live-Cell Imaging of NPC Dynamics in the Ventral Spinal Cord. To observe engrafted NPC behavior, GFP-NPCs were transplanted intraspinally at thoracic vertebra 10 (5, 24, 29) and were monitored ex vivo under 2P excitation. We first confirmed that GFP-fluorescent cells were indeed NPCs and that the fluorescence did not arise from other cells that may have phagocytosed GFP-NPCs. Spinal cord slices were stained for the ionized calcium-binding adaptor molecule 1 (Iba-1), a marker of activated macrophages and microglia (30). Despite a high number of activated macrophages and microglia in the spinal cord 3 wk following transplant, GFP fluorescence did not overlap with Iba-1 staining (Fig. 3*A*), demonstrating that the GFP fluorescence observed in the spinal cord was not due to engulfed NPCs and this was consistent with earlier studies (5).

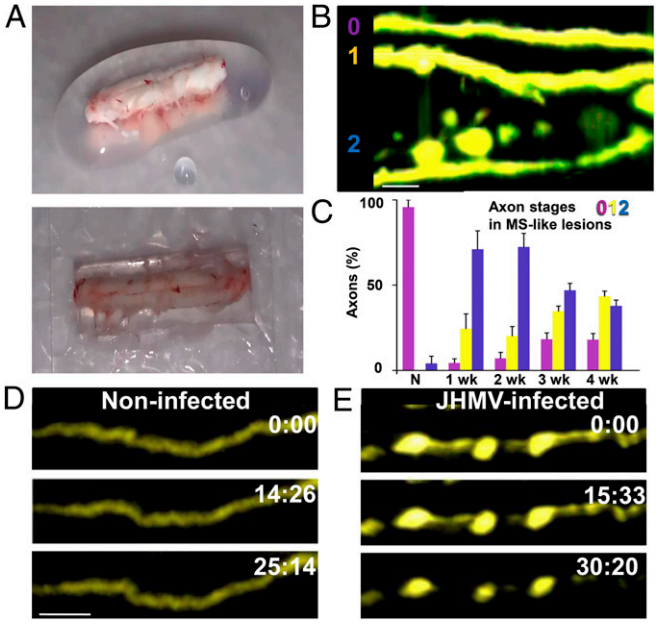

Fig. 1. Focal axonal degeneration occurs in the ventral side of JHMV-infected Thy1-YFP mouse spinal cords. (*A*) An explanted mouse spinal cord embedded in a 5% agarose gel (*Upper*) and mounted on a coverslip with the ventral surface exposed before 2P imaging (*Lower*). (*B*) Representative image illustrating multiple stages of FAD (0, 1, 2, as indicated) in the ventral side of a Thy1-YFP (yellow) spinal cord 21 d following JHMV infection. (*C*) Proportions of axons (% ± SEM) displaying different FAD stages in normal spinal cord (N) and in lesioned regions 1–4 wk after JHMV infection; differences at all time points compared with control are significant, $P < 0.001$–0.05. (*D*) Time-lapse images (times marked in min:s) depicting absence of FAD in a noninfected Thy1-YFP spinal cord. (*E*) Time-lapse images showing progression of FAD in a Thy1-YFP spinal cord 7 d following JHMV infection (Movie S1). (Scale bars in *B*, *D*, and *E*, 20 μm.)

At day 1 following GFP-NPC transplantation into a noninfected mouse, clusters of cells had limited motility at the site of transplant (Fig. S1A). In control noninfected mice, GFP-NPCs moved with an average velocity of 1.9 ± 0.1 $\mu m \cdot min^{-1}$ ($n = 5$). NPC motility characteristics were altered in the JHMV-infected demyelinated spinal cord, where GFP-NPCs moved with a lower average velocity of 0.9 ± 0.05 $\mu m \cdot min^{-1}$ at the transplant site ($n = 6$) (Fig. S1B). In contrast to the limited motility observed at the injection site, GFP-NPCs located 300 μm or farther from the transplant site were observed to move more rapidly in both infected and noninfected mice. (Fig. 3*B* and Movie S2). At day 1 posttransplant, GFP-NPCs were observed distal to the transplant site in three of five noninfected and three of six JHMV-infected mice. GFP-NPCs >300 μm from the transplant site had an average velocity of 5.0 ± 0.7 $\mu m \cdot min^{-1}$ in the JHMV-infected spinal cord, compared with 9.3 ± 0.6 $\mu m \cdot min^{-1}$ in the noninfected spinal cord (Fig. 3*C*). We applied directional persistence analysis (31) to further characterize NPC migration to describe the direction of cell movement over time; a value of 1 represents migration along a straight line without turning, 0 represents neutral

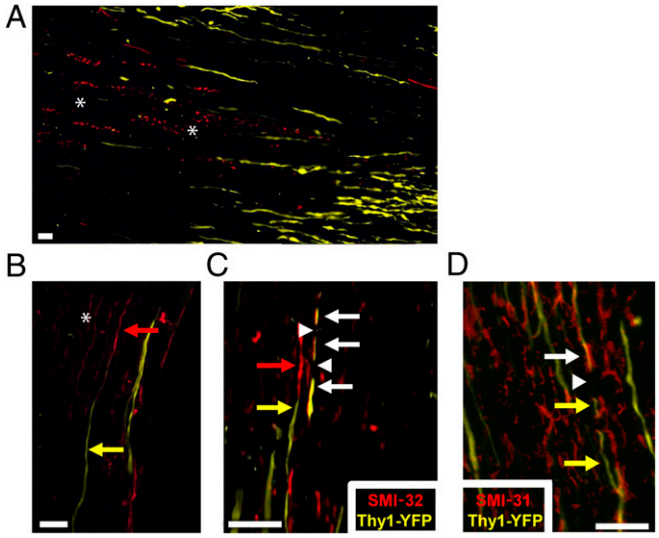

Fig. 2. Loss of YFP signal correlates with axonal damage in both intact and transected axonal regions. (*A*) Spinal cord section from a Thy1-YFP mouse imaged 23 d p.i. by immunofluorescence microscopy, colabeled with α-SMI-32 (red) to show damaged axons. White asterisks indicate lesions with multiple SMI-32$^+$ damaged axons. (*B*) Loss of YFP signal does not necessarily indicate axonal transection. Fluorescence image shows axonal regions without damage (yellow arrow, YFP$^+$SMI-32$^-$) and damaged axonal regions without YFP signal (red arrow, YFP$^-$SMI-32$^+$). White asterisk represents a lesion with multiple SMI-32$^+$ axons. (*C*) Example of complete axonal transections (white arrowheads, YFP$^-$SMI-32$^-$) in an axon with intact damaged regions with YFP signal (white arrows, YFP$^+$SMI-32$^+$). (*D*) Fluorescence image shows YFP$^+$ axonal regions without damage (white arrow, YFP$^+$SMI-31$^+$), damaged axonal regions with YFP signal (yellow arrow, YFP$^+$SMI-31$^-$), and damaged/transected axonal regions without YFP signal (white arrowhead, YFP$^-$SMI-31$^-$). (Scale bars, 20 μm.)

movement, and −1 represents migration directly toward the track origin (*Methods*). The directional persistence of transplanted NPCs was significantly lower in the JHMV-infected spinal cord, compared with the noninfected spinal cord (Fig. 3*C*).

When examined 14 d after transplant, GFP-NPCs were observed in dense clusters in the ventral area of the thoracic region of both the noninfected and the JHMV-infected spinal cord. A subset of GFP-NPCs expressed Ki-67, a nuclear marker of cellular proliferation (32), indicating proliferation occurred 2 wk after transplant (Fig. 4*A*). Proliferation was significantly increased within the JHMV-infected spinal cord, in which 55.7 ± 6.8% of DAPI$^+$ GFP-NPCs expressed Ki-67, compared with 14.4 ± 2.2% in the noninfected spinal cord (Fig. 4*B*). Two-photon imaging revealed that GFP-NPCs exhibit dynamic morphologies in the ventral spinal cord. Cells were observed to proliferate, with large (~10 μm) "buds" protruding off clusters of GFP-NPCs (Fig. 4*C* and Movie S3), and GFP-NPCs actively extended and retracted processes in both the noninfected and the JHMV-infected spinal cord (Fig. S2 and Movie S4).

GFP-NPCs Preferentially Colocalize with Damaged Axons. One week following NPC transplantation into the JHMV-infected Thy1-YFP mouse, GFP-NPCs closely associated with stage 1 and stage 2 FAD axons (Fig. 5 *A* and *B*). Large clusters of GFP-NPCs preferentially established residence in regions with extensive axonal damage as determined by the FAD index (Fig. 5*C*). Following migration to FAD lesions, GFP-NPCs initiated intercellular interactions with stage 1 and stage 2 FAD axons (Fig. 5*D* and Movie S5), gathering YFP fluorescent segments of stage 2 axons together (Fig. 5*E* and Movie S6). Because loss of YFP signal does not necessarily indicate a transected axon, GFP-NPC contact with an axon may alter YFP fluorescence within intact FAD axons. Therefore, we examined GFP-NPCs that transiently contacted Thy1-YFP axons at 2 wk posttransplant. Axonal pathology has been associated with a decrease in YFP fluorescence (20), suggesting that NPC interactions with FAD axons may stabilize axons. In transient interactions, as the colocalization of an NPC and an axon diminished, YFP fluorescence rapidly decreased in the axon, changing the axon from FAD 1 to FAD 2 (Fig. 6 *A*–*C* and Movie S7). Analysis of multiple GFP-NPCs revealed that the migration of NPCs away from damaged axons was strongly correlated with the loss of axonal YFP fluorescence (Fig. 6*D*).

Engrafted GFP-NPCs Remyelinate Axons. To determine whether transplanted NPCs produce myelin following interactions with damaged axons, we cultured NPC neurospheres isolated from mice that express GFP under the control of the myelin proteolipid protein promoter (PLP-GFP) (33). Two weeks following transfer into a JHMV-infected spinal cord, NPCs formed stable interactions with damaged axons and expressed GFP, indicating that transplanted NPCs differentiated into myelinating cells and expressed myelin genes (Fig. 7*A*). In these cells, GFP fills the cytoplasm of the cell body, revealing that differentiated NPCs wrapped around damaged axons (Movie S8), with the GFP fluorescence extending around the length of the axon (Fig. 7*B*). Correspondingly, YFP fluorescence increased (Fig. 7*C*), indicating increased axonal health based on earlier reports correlating axonal health/integrity with YFP expression (20). Furthermore, we found GFP-NPCs wrapped around YFP$^+$ axons and myelin basic protein (MBP)

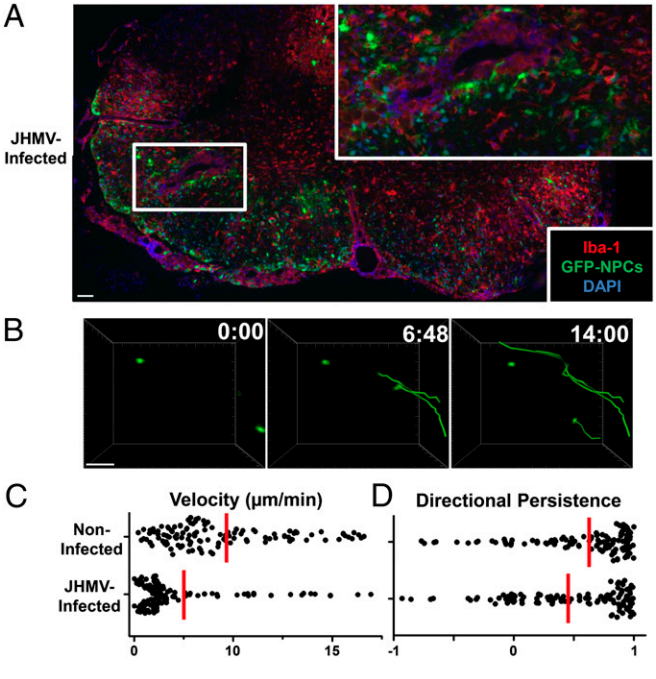

Fig. 3. GFP-NPC motility in the spinal cord 1 d posttransfer. (*A*) Immunohistochemistry illustrating localization of mouse GFP-NPCs (green) in the spinal cord of a C57BL/6 mouse 3 wk posttransfer. Activated microglia and macrophages labeled with anti-ionized calcium-binding adapter molecule 1 (Iba-1) are shown in red, overlaid with DAPI-stained nuclei (blue). *Inset* shows a separation of green and red fluorescence in the enlarged area. (*B*) Time-lapse two-photon image in an explanted noninfected C57BL/6 spinal cord, showing transferred GFP-NPC (green) motility distal from the transplant site 1 d posttransfer. Panels depict cell positions at the times indicated (min:s), together with superimposed tracks showing movement beginning at 0:00 (Movie S2). (Scale bars, 40 μm.) (*C*) Distribution of instantaneous GFP-NPC cellular velocities in the spinal cord of a C57BL/6 mouse 1 d posttransfer. Overall mean is indicated in red ($P < 0.0001$). (*D*) Scatter plot of GFP-NPC directional persistence (dp) in the spinal cord (noninfected, dp = 0.62 ± 0.03; JHMV-infected, dp = 0.48 ± 0.04; $P = 0.027$).

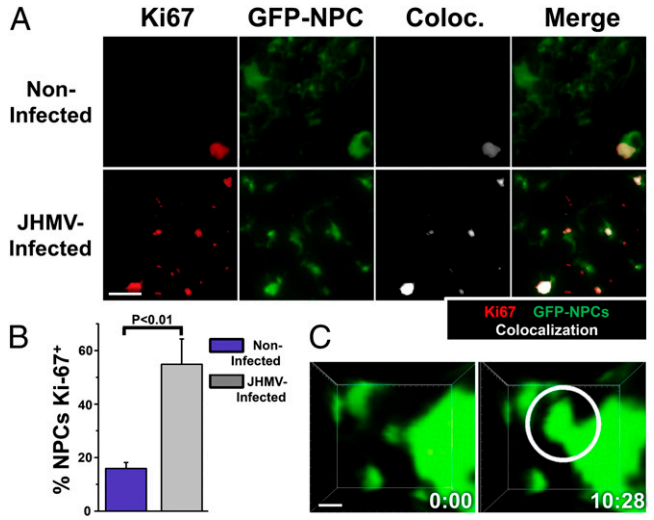

Fig. 4. GFP-NPCs proliferate extensively in the JHMV-infected spinal cord. (*A*) Immunostaining in transverse sections of JHMV-infected spinal cords 2 wk after GFP-NPC transplantation. Ki-67 (red), GFP-NPCs (green), and colocalization between overlapping GFP-NPC and Ki-67 fluorescence were determined using the Imaris colocalization tool (white). (*Right*) Merge of all three channels. (*B*) Quantification of the number of Ki-67^{+}GFP^{+} nuclei divided by the number of DAPI^{+}GFP^{+} nuclei in multiple spinal cord sections from transplanted mice. (*C*) Time-lapse images of a GFP-NPC cluster expanding at the indicated time points (min:s) in a noninfected spinal cord 7 d posttransfer (Movie S3). (Scale bars, 10 μm.)

colocalized with GFP fluorescence, further confirming that transplanted NPCs actively participate in remyelination (Fig. 7*D* and Fig. S3).

Discussion

Our results indicate that transplanted GFP-NPCs preferentially migrate to regions of axonal damage, proliferate, and actively remyelinate axons. NPCs have been shown to selectively colonize areas of white matter damage and facilitate remyelination in preclinical animal models of neuroinflammatory demyelination (5, 8, 34, 35). However, the migration of transplanted NPCs and their interactions with damaged axons has not previously been visualized. In this study, we established a system for stable ex vivo imaging to observe single NPC behavior in the ventral spinal cords of mice, using a model of viral-induced demyelination. Although the etiology of MS is unknown, numerous factors including both genetic and environmental influences are considered important in initiation and maintenance of disease. Viral infection has long been considered a potential triggering mechanism involved in demyelination, and numerous human viral pathogens have been suggested to be involved in eliciting myelin-reactive lymphocytes and/or antibodies that subsequently infiltrate the CNS and damage the myelin sheath (36–39). As such, viral models of neuroinflammation/demyelination are relevant and have provided important insights into mechanisms associated with disease. Moreover, the molecular mechanisms governing how engrafted NPCs interact with demyelinated axons within an inflammatory environment resulting from demyelination derived from a persistent viral infection have not been defined. Therefore, the present study uses the JHMV model of demyelination to characterize NPC migration kinetics as well as their ability to physically engage demyelinated axons and promote remyelination. To accomplish this, we used transgenic Thy1-YFP mice and 2P microscopy to visualize axonal damage following JHMV infection and imaged real-time interactions of transplanted GFP-NPCs with damaged axons, allowing insight into mechanisms by which transplanted NPCs contribute to amelioration of clinical and histopathological disease.

Axonal damage in MS is considered a secondary event that occurs following myelin loss in response to accumulation of myelin-reactive lymphocytes within the CNS and this is supported by experimental autoimmune encephalomyelitis (EAE), an autoimmune model of neuroinflammation and demyelination. More recently, through use of viral models of demyelination as well as EAE, emerging evidence supports the possibility that axonal damage precedes demyelination (40–44). Within 1 wk following infection of Thy1-YFP mice with JHMV, we observed axons with FAD, characterized by discontinuous YFP fluorescence, consistent with earlier reports describing axonopathy in JHMV-infected mice (41, 45). Our findings indicate that axonal damage occurs early following JHMV infection of the CNS before robust immune-mediated demyelination. Previous in vivo imaging studies of the demyelinated spinal cord suggest that loss of fluorescence in axons indicates total axonal transection (20, 23). However, we show that loss of YFP fluorescence can occur in an intact axon and does not necessarily mean axonal transection. Although it is possible a variety of cell types may interact with axonal segments, we show that axonal YFP fluorescence changes reversibly during and subsequent to interaction with transplanted NPCs, judged by colocalization with transplanted NPCs. The observed variability in the amount of axonal YFP fluorescence change may be a result of the extent of axonal damage at the time of interaction or the length of the imaging window. These results extend previous studies from our laboratory that demonstrated axonal sparing following NPC transplantation into JHMV-infected mice (8).

Physical engagement of damaged axons by transplanted NPCs increases axonal YFP fluorescence, and disengagement of NPCs

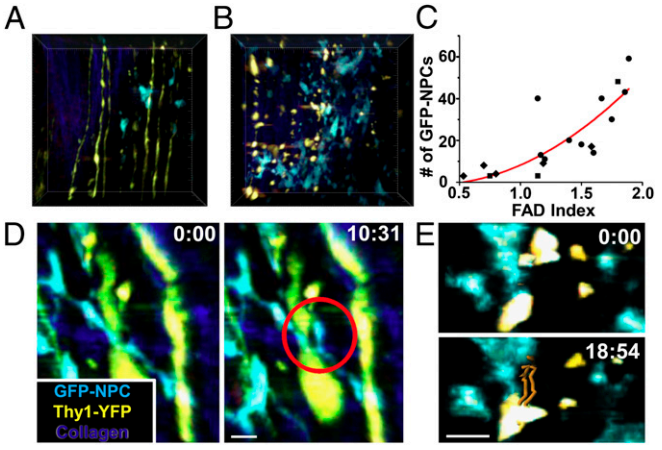

Fig. 5. GFP-NPCs colocalize and initiate intercellular interactions with damaged axons. (*A*) Representative image showing colocalization between GFP-NPCs (teal) and "stage 1 FAD" axons (yellow) in the JHMV-infected Thy1-YFP spinal cord 8 d posttransfer. Endogenous spinal cord structures (collagen) are visualized by second harmonic generation (blue). (*B*) Representative image from the same spinal cord as in *A*, showing increased colocalization between GFP-NPCs and "stage 2 FAD" axons in a more damaged lesion in the JHMV-infected Thy1-YFP spinal cord 8 d posttransfer. (*C*) GFP-NPC localization correlates with the FAD severity of lesions in the JHMV-infected Thy1-YFP spinal cord 8 d posttransfer. Number of transferred GFP-NPCs found in lesions is plotted vs. FAD severity of the lesions for each 10^{-5} cm^{3} imaging volume. FAD index is calculated as described in *Methods*. Multiple lesions in three separate mice are shown, with different symbols (■, ●, ♦) representing each mouse with the polynomial fit in red. Correlation coefficient (*r*): 0.78. (*D*) Time-lapse images showing GFP-NPCs initiating intercellular interactions with stage 1 FAD axons in the JHMV-infected Thy1-YFP spinal cord 8 d posttransfer. Circle indicates a GFP-NPC actively extending a process toward the axon (Movie S5). (*E*) GFP-NPCs bring together YFP-fluorescent axonal segments in JHMV-infected Thy1-YFP spinal cord. Panels depict cell positions at the times indicated, together with superimposed tracks depicting progressive YFP migration since the beginning of the record (Movie S6). (Scale bars, 10 μm.)

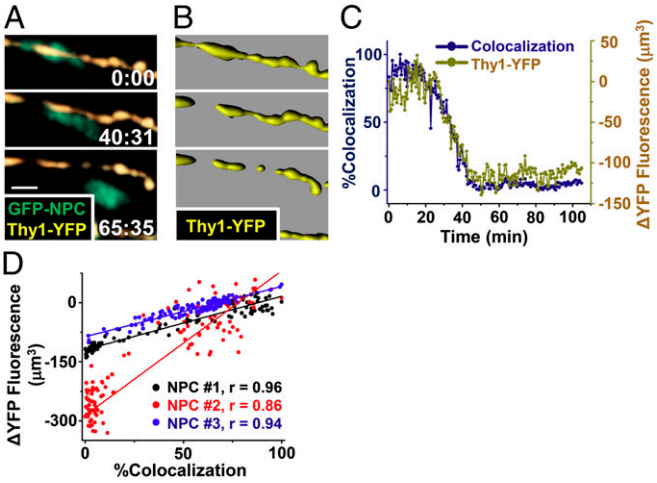

Fig. 6. GFP-NPC colocalization with damaged Thy1-YFP$^+$ axons determines axonal YFP fluorescence. (*A*) Time-lapse images showing a GFP-NPC (green) migrating away from a FAD Thy1-YFP$^+$ axon (yellow) in a JHMV-infected Thy1-YFP spinal cord 14 d posttransfer (Movie S7). (Scale bar, 10 μm.) (*B*) Imaris analysis of the axonal fluorescence depicted in *A* with Thy1-YFP pixel volume represented in yellow. (*C*) Quantification of GFP-NPC and Thy1-YFP colocalization (left axis) and change in axonal Thy1-YFP fluorescence (right axis, normalized to starting fluorescence) during the imaging period. Colocalization between overlapping GFP-NPC and Thy1-YFP fluorescence in the imaging field was determined using the Imaris colocalization tool, and the fluorescence of Thy1-YFP axons in the imaging field was determined by the Imaris Surfaces tool. Maximum colocalization of GFP and YFP fluorescence is defined as 100% colocalization. (*D*) Analysis of three different representative GFP-NPC and Thy1-YFP colocalizations and change in axonal Thy1-YFP fluorescence, where each data point represents a time point for that particular interaction. The linear regression for each dataset is shown. Correlation coefficients (*r*): 0.92 ± 0.03, $n = 3$.

from axons rapidly diminishes YFP signal intensity. Loss of YFP fluorescence may occur in intact axons due to impaired microtubular transport (46), axonal swelling resulting in retraction of proteins from damaged areas (47), changes in reactive oxygen and nitrogen species that initiate mitochondrial pathology (48), or changes in ion channel expression (49) that do not allow for a favorable environment for YFP fluorescence. However, to account for the rapid changes in YFP fluorescence, we propose that interactions with NPCs may reverse acidification and diminish elevated internal calcium concentrations present in axons in inflammatory lesions through effects on NMDA receptors (23) or acid-sensing ion channels (50). YFP fluorescence is particularly sensitive to acidic pH (51), indicating that restoration of normal physiological pH may underlie rapid increases in axonal YFP fluorescence observed during remyelination. Continued studies examining these possibilities are required to better understand the nature of axonal damage in response to CNS viral infection and the ability of NPCs to protect and repair damaged axons.

We have previously shown that transplanted GFP-NPCs preferentially colonize areas of demyelination and this positional migration is guided, in part, by expression of the chemokine receptor CXCR4 on transplanted NPCs that respond to enriched expression of the chemokine ligand CXCL12 that is enriched within areas of white matter pathology (5). However, the motility of engrafted NPCs was not examined. Our results support and extend those earlier findings by showing that NPCs recognize and directly interact with damaged axons. Further, we now demonstrate motility differences between NPCs transplanted into a demyelinated spinal cord and NPCs transplanted into a non-infected spinal cord. One day following transplant into the JHMV-infected spinal cord, the motility of GFP-NPCs was slower than in the absence of infection. This result may be due to GFP-NPCs initiating contact with demyelinated axons. In support of this, we demonstrate that transplanted GFP-NPCs extended processes and make extensive contacts with damaged axons. However, it is possible that reduced GFP-NPC motility is due to inflammatory signals in the JHMV-infected spinal cord. The molecular signals mediating this interaction are to this point undefined, although previous studies have clearly shown that NPCs are capable of expressing adhesion molecules that may engage axons (52).

Engagement of damaged axons by transplanted GFP-NPCs is the first step in events leading to NPC differentiation and remyelination (53, 54). We have previously shown that the majority of transplanted NPCs into JHMV-infected mice differentiate into oligodendroglia, the myelinating cells of the CNS supporting an important role for transplanted cells in participating in remyelination (5, 8). Moreover, transplantation of NPCs lacking the transcription factor *Olig1* into JHMV-infected mice results in diminished clinical and histologic recovery that correlates with altered lineage fate commitment as *Olig1*-deficient NPCs preferentially differentiate into astrocytes (55). Until now, studies have shown that transplanted NPCs directly or indirectly contribute to endogenous remyelination (11, 55), although evidence of direct remyelination

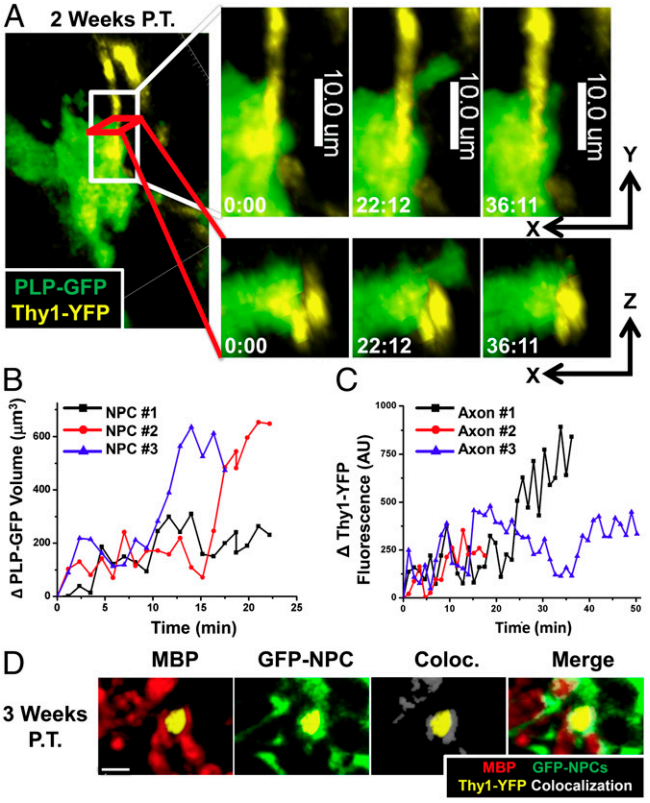

Fig. 7. Transplanted NPCs expressing cytoplasmic GFP driven by the myelin proteolipid protein (PLP) promoter wrap around damaged axons. (*A*) Representative image showing colocalization between PLP-GFP (green) and stage 1 FAD axons (yellow) in the JHMV-infected Thy1-YFP spinal cord 15 d posttransfer. (*Right*) Enlarged time-lapse images of a PLP-GFP–positive cell wrapping around an axon (min:s). (*Upper*) *x-y* sections; (*Lower*) *x-z* sections (Movie S8). (*B*) Analysis of the change in volume of PLP-GFP fluorescence of three different NPCs during wrapping as determined by a time-lapse 3D reconstruction of the 2P data and the Imaris "Surfaces" tool. (*C*) Analysis of the change in Thy1-YFP fluorescence intensity during PLP-GFP wrapping presented as arbitrary fluorescent units (AU). (*D*) Immunostaining in a transverse section of a JHMV-infected Thy1-YFP spinal cord 21 d after GFP-NPC transplantation. MBP (red), YFP$^+$ axons (yellow), and colocalization between overlapping GFP-NPC (green) and MBP fluorescence were determined using the Imaris colocalization tool (white). (*Right*) Merge of all three channels. (Scale bar, 4 μm.)

was not entirely conclusive. Whereas we have previously shown that GFP expression from transplanted NPCs colocalized with MBP (55), our real-time imaging of PLP-expressing NPCs definitively demonstrates that transplanted NPCs directly remyelinate axons and are not merely stimulating endogenous oligodendroglia to remyelinate. We show that NPC-derived oligodendrocytes express PLP, a protein necessary for myelination, and extend and cover axons within ~20 min. Finally, this study also provides a model system to better understand the physical nature of NPC interactions with damaged axons.

Methods

Mice and Virus. C57BL/6 (National Cancer Institute) and Thy1-YFP (25) (Jackson Laboratory) mice were infected intracranially (i.c.) with 150 plaque-forming units (PFU) of JHMV strain J2.2v-1 (JHMV) in 30 μL sterile Hanks' balanced saline solution (HBSS) (5, 24). Mice were killed by inhalation of halothane (Sigma-Aldrich) at various days postinfection (p.i.), and spinal cords were removed and processed for analysis. For tissues used for immunohistochemistry, mice were fixed by cardiac profusion. Mice expressing eGFP driven by the mouse myelin PLP gene promoter were used to generate NPCs that express eGFP only, following terminal differentiation into mature myelinating oligodendrocytes (33). All experiments were approved by the University of California, Irvine, Institutional Animal Care and Use Committee.

Cell Culture, Reagents, and Transplantation. Enhanced green fluorescent protein-expressing NPCs (GFP-NPCs), derived from C57BL/6 mice, were cultured as previously described (24). In addition, NPCs from PLP-GFP mice were isolated and cultured before transplantation as previously described (34, 55). Following culture in DMEM:F12 (Invitrogen) supplemented with 1× B27 (Invitrogen), 1× insulin–transferrin–selenium (Invitrogen), 1× penicillin–streptomycin (Invitrogen), 40 ng/mL T3 (Sigma-T67407), and 20 ng/mL human recombinant EGF (Sigma-E9644) for 5 d, PLP-GFP neurospheres were dissociated with 1× TrypLE (Gibco-12563-011) for 20 min at 37 °C and centrifuged for 5 min at 500 × *g*, 4 °C. Cells were resuspended and triturated in 1× HBSS followed by three washes with 1× HBSS. Undifferentiated GFP-NPCs or PLP-GFP-NPCs were transplanted (2.5×10^5 in 2.5 μL HBSS per mouse) at spinal cord T10 at day 14 p.i. into C57BL/6 and Thy1-YFP mice. As previously published, this time point for transplantation was chosen because virus and inflammation have waned whereas demyelination has peaked (5).

Spinal Cord Preparation, Two-Photon Imaging, and Analysis. Two-photon imaging was performed using a previously described system (56) with a Chameleon Ultra II Ti:Sapphire laser (Coherent). Spinal cords were isolated from thoracic vertebra 4 to lumbar vertebra 2, embedded in a 5% agarose gel to maintain the integrity of the spinal cord, oriented with the ventral side facing the dipping objective, and superfused with warmed, oxygenated medium as applied for ex vivo imaging of other explanted organs (56). Explanted spinal cords were imaged with a laser excitation of 900 nm. Five hundred twenty- and 560-nm dichroic mirrors (Semrock) separated emission into blue (<520 nm), green (520–560 nm), and red (>560 nm) channels. Imaging volumes of $x = 270$ μm, $y = 212$ μm, and $z = 100$ μm were acquired using Slidebook version 4.2 and 3D stacks were compiled in Metamorph version 6.1 (Molecular Devices). Imaging analysis was performed in Imaris version 7.3 (Bitplane). Increased power to the blue channel photomultiplier tube and Gaussian filtering were applied to improve visual separation of eGFP and eYFP. In final videos, cells were pseudocolored to enhance color separation between eYFP and eGFP. To calculate directional persistence we used the equation

$$dp = (D_2 - D_1) + \frac{D_3 - D_2}{d_2 + d_3},$$

where D equals displacement and d equals distance, which was calculated every two steps for sequential 3D coordinates of cell position (31). FAD index of MS-like lesions was calculated based on an axonal degradation index previously described (20):

$$\text{FAD index} = \frac{[(\#\text{ of stage 1 axons} \cdot 1) + (\#\text{ of stage 2 axons} \cdot 2)]}{\#\text{ axons}}.$$

Immunohistochemistry. The murine spinal cord was extracted and processed for optimal cutting temperature compound and resin-embedded sections as previously described (8). For immunofluorescence staining, slides were prepared and blocked with goat serum in 1× PBS + 0.5% BSA as previously described (8). Primary antibodies included rabbit anti-Iba1 (1 mg/mL; Wako Chemicals), rabbit anti-MBP (1:200; Chemicon), mouse anti-SMI-31 (phosphorylated neurofilament H; 1:1,000; EMD Millipore), or mouse anti-SMI-32 (nonphosphorylated neurofilament H; 1:1,000; Covance). Anti-SMI-31 and anti-SMI-32 were blocked as described above with the addition of 5% (vol/vol) purified goat anti-mouse IgG (Invitrogen). The secondary antibody used for anti-Iba1 and anti-MBP was Alexa 594 goat anti-rabbit (1:1,000; Invitrogen); for anti-SMI-31 and anti-SMI-32, Alexa 594 goat anti-mouse (1:1,000; Invitrogen) was used. DAPI Fluoromount-G (Southern Biotech) was used to visualize nuclei. Colocalization of overlapping fluorescence was determined using Imaris 7.3 (Bitplane). Pixel intensities over a set threshold at the same position were considered colocalized.

Statistical Analysis. Statistical significance for velocity measurements in Fig. 3*C* was determined using Student's *t* test. The Mann–Whitney *U* test was used to calculate significance for the nonnormally distributed directional persistence measurements in Fig. 3*D*. A P value <0.05 was considered significant. Data are presented as mean ± SEM.

ACKNOWLEDGMENTS. We acknowledge the California Institute for Regenerative Medicine core facilities at the University of California, Irvine. This work was supported in part by National Institutes of Health (NIH) Grants R01 GM-41514 (to M.D.C.) and R01 NS-074987 (to T.E.L.) and the National Multiple Sclerosis Society (NMSS) Collaborative Center Research Award CA1058-A-8 (to T.E.L. and M.D.C.), NMSS Grant RG4925, NIH Training Grant T32-AI-060573 (to M.L.G.), and NMSS Postdoctoral Fellowship FG 1960-A-1 (to J.G.W.).

1. Compston A, Coles A (2008) Multiple sclerosis. *Lancet* 372(9648):1502–1517.
2. Miller DJ, Rodriguez M (1995) Spontaneous and induced remyelination in multiple sclerosis and the Theiler's virus model of central nervous system demyelination. *Microsc Res Tech* 32(3):230–245.
3. Palmer AM (2009) Pharmacotherapy for multiple sclerosis: Progress and prospects. *Curr Opin Investig Drugs* 10(5):407–417.
4. Bai L, Hecker J, Kerstetter A, Miller RH (2013) Myelin repair and functional recovery mediated by neural cell transplantation in a mouse model of multiple sclerosis. *Neurosci Bull* 29(2):239–250.
5. Carbajal KS, Schaumburg C, Strieter R, Kane J, Lane TE (2010) Migration of engrafted neural stem cells is mediated by CXCL12 signaling through CXCR4 in a viral model of multiple sclerosis. *Proc Natl Acad Sci USA* 107(24):11068–11073.
6. Karimi-Abdolrezaee S, Eftekharpour E, Wang J, Morshead CM, Fehlings MG (2006) Delayed transplantation of adult neural precursor cells promotes remyelination and functional neurological recovery after spinal cord injury. *J Neurosci* 26(13):3377–3389.
7. Mothe AJ, Tator CH (2008) Transplanted neural stem/progenitor cells generate myelinating oligodendrocytes and Schwann cells in spinal cord demyelination and dysmyelination. *Exp Neurol* 213(1):176–190.
8. Totoiu MO, Nistor GI, Lane TE, Keirstead HS (2004) Remyelination, axonal sparing, and locomotor recovery following transplantation of glial-committed progenitor cells into the MHV model of multiple sclerosis. *Exp Neurol* 187(2):254–265.
9. Gupta N, et al. (2012) Neural stem cell engraftment and myelination in the human brain. *Sci Transl Med* 4(155):155ra137.
10. Lu P, et al. (2012) Long-distance growth and connectivity of neural stem cells after severe spinal cord injury. *Cell* 150(6):1264–1273.
11. Einstein O, Friedman-Levi Y, Grigoriadis N, Ben-Hur T (2009) Transplanted neural precursors enhance host brain-derived myelin regeneration. *J Neurosci* 29(50):15694–15702.
12. Bender SJ, Weiss SR (2010) Pathogenesis of murine coronavirus in the central nervous system. *J Neuroimmune Pharmacol* 5(3):336–354.
13. Bergmann CC, Lane TE, Stohlman SA (2006) Coronavirus infection of the central nervous system: Host-virus stand-off. *Nat Rev Microbiol* 4(2):121–132.
14. Hosking MP, Lane TE (2010) The role of chemokines during viral infection of the CNS. *PLoS Pathog* 6(7):e1000937.
15. Stohlman SA, Hinton DR (2001) Viral induced demyelination. *Brain Pathol* 11(1):92–106.
16. Templeton SP, Perlman S (2007) Pathogenesis of acute and chronic central nervous system infection with variants of mouse hepatitis virus, strain JHM. *Immunol Res* 39(1–3):160–172.
17. Hardison JL, Nistor G, Gonzalez R, Keirstead HS, Lane TE (2006) Transplantation of glial-committed progenitor cells into a viral model of multiple sclerosis induces remyelination in the absence of an attenuated inflammatory response. *Exp Neurol* 197(2):420–429.
18. Germain RN, Robey EA, Cahalan MD (2012) A decade of imaging cellular motility and interaction dynamics in the immune system. *Science* 336(6089):1676–1681.
19. Kim JV, et al. (2010) Two-photon laser scanning microscopy imaging of intact spinal cord and cerebral cortex reveals requirement for CXCR6 and neuroinflammation in immune cell infiltration of cortical injury sites. *J Immunol Methods* 352(1–2):89–100.
20. Nikić I, et al. (2011) A reversible form of axon damage in experimental autoimmune encephalomyelitis and multiple sclerosis. *Nat Med* 17(4):495–499.

21. Nitsch R, et al. (2004) Direct impact of T cells on neurons revealed by two-photon microscopy in living brain tissue. *J Neurosci* 24(10):2458–2464.
22. Odoardi F, et al. (2012) T cells become licensed in the lung to enter the central nervous system. *Nature* 488(7413):675–679.
23. Siffrin V, et al. (2010) In vivo imaging of partially reversible th17 cell-induced neuronal dysfunction in the course of encephalomyelitis. *Immunity* 33(3):424–436.
24. Weinger JG, et al. (2012) MHC mismatch results in neural progenitor cell rejection following spinal cord transplantation in a model of viral-induced demyelination. *Stem Cells* 30(11):2584–2595.
25. Feng G, et al. (2000) Imaging neuronal subsets in transgenic mice expressing multiple spectral variants of GFP. *Neuron* 28(1):41–51.
26. Kerschensteiner M, Schwab ME, Lichtman JW, Misgeld T (2005) In vivo imaging of axonal degeneration and regeneration in the injured spinal cord. *Nat Med* 11(5): 572–577.
27. Campbell MJ, Morrison JH (1989) Monoclonal antibody to neurofilament protein (SMI-32) labels a subpopulation of pyramidal neurons in the human and monkey neocortex. *J Comp Neurol* 282(2):191–205.
28. Sánchez I, et al. (2000) Local control of neurofilament accumulation during radial growth of myelinating axons in vivo. Selective role of site-specific phosphorylation. *J Cell Biol* 151(5):1013–1024.
29. Carbajal KS, Miranda JL, Tsukamoto MR, Lane TE (2011) CXCR4 signaling regulates remyelination by endogenous oligodendrocyte progenitor cells in a viral model of demyelination. *Glia* 59(12):1813–1821.
30. Ito D, et al. (1998) Microglia-specific localisation of a novel calcium binding protein, Iba1. *Brain Res Mol Brain Res* 57(1):1–9.
31. Matheu MP, et al. (2012) Toll-like receptor 4-activated B cells out-compete Toll-like receptor 9-activated B cells to establish peripheral immunological tolerance. *Proc Natl Acad Sci USA* 109(20):E1258–E1266.
32. Gerdes J, Schwab U, Lemke H, Stein H (1983) Production of a mouse monoclonal antibody reactive with a human nuclear antigen associated with cell proliferation. *Int J Cancer* 31(1):13–20.
33. Mallon BS, Shick HE, Kidd GJ, Macklin WB (2002) Proteolipid promoter activity distinguishes two populations of NG2-positive cells throughout neonatal cortical development. *J Neurosci* 22(3):876–885.
34. Ben-Hur T, Rogister B, Murray K, Rougon G, Dubois-Dalcq M (1998) Growth and fate of PSA-NCAM+ precursors of the postnatal brain. *J Neurosci* 18(15):5777–5788.
35. Pluchino S, et al. (2003) Injection of adult neurospheres induces recovery in a chronic model of multiple sclerosis. *Nature* 422(6933):688–694.
36. Ascherio A, Munger KL (2007) Environmental risk factors for multiple sclerosis. Part I: The role of infection. *Ann Neurol* 61(4):288–299.
37. Ascherio A, Munger KL (2007) Environmental risk factors for multiple sclerosis. Part II: Noninfectious factors. *Ann Neurol* 61(6):504–513.
38. Ebers GC, Sadovnick AD, Risch NJ; Canadian Collaborative Study Group (1995) A genetic basis for familial aggregation in multiple sclerosis. *Nature* 377(6545):150–151.
39. Sospedra M, Martin R (2005) Immunology of multiple sclerosis. *Annu Rev Immunol* 23: 683–747.
40. Das Sarma J (2010) A mechanism of virus-induced demyelination. *Interdiscip Perspect Infect Dis* 2010:109239.
41. Das Sarma J, Kenyon LC, Hingley ST, Shindler KS (2009) Mechanisms of primary axonal damage in a viral model of multiple sclerosis. *J Neurosci* 29(33):10272–10280.
42. Geurts JJ, Kooi EJ, Witte ME, van der Valk P (2010) Multiple sclerosis as an "inside-out" disease. *Ann Neurol* 68(5):767–768, author reply 768.
43. Sato F, Tanaka H, Hasanovic F, Tsunoda I (2011) Theiler's virus infection: Pathophysiology of demyelination and neurodegeneration. *Pathophysiology* 18(1):31–41.
44. Tsunoda I, Tanaka T, Saijoh Y, Fujinami RS (2007) Targeting inflammatory demyelinating lesions to sites of Wallerian degeneration. *Am J Pathol* 171(5):1563–1575.
45. Dandekar AA, Wu GF, Pewe L, Perlman S (2001) Axonal damage is T cell mediated and occurs concomitantly with demyelination in mice infected with a neurotropic coronavirus. *J Virol* 75(13):6115–6120.
46. Tang-Schomer MD, Johnson VE, Baas PW, Stewart W, Smith DH (2012) Partial interruption of axonal transport due to microtubule breakage accounts for the formation of periodic varicosities after traumatic axonal injury. *Exp Neurol* 233(1): 364–372.
47. Byun N, Delpire E (2007) Axonal and periaxonal swelling precede peripheral neurodegeneration in KCC3 knockout mice. *Neurobiol Dis* 28(1):39–51.
48. Campbell GR, Mahad DJ (2012) Mitochondrial changes associated with demyelination: Consequences for axonal integrity. *Mitochondrion* 12(2):173–179.
49. Black JA, Newcombe J, Trapp BD, Waxman SG (2007) Sodium channel expression within chronic multiple sclerosis plaques. *J Neuropathol Exp Neurol* 66(9):828–837.
50. Friese MA, et al. (2007) Acid-sensing ion channel-1 contributes to axonal degeneration in autoimmune inflammation of the central nervous system. *Nat Med* 13(12):1483–1489.
51. Llopis J, McCaffery JM, Miyawaki A, Farquhar MG, Tsien RY (1998) Measurement of cytosolic, mitochondrial, and Golgi pH in single living cells with green fluorescent proteins. *Proc Natl Acad Sci USA* 95(12):6803–6808.
52. Kokovay E, et al. (2012) VCAM1 is essential to maintain the structure of the SVZ niche and acts as an environmental sensor to regulate SVZ lineage progression. *Cell Stem Cell* 11(2):220–230.
53. Baron W, Colognato H, ffrench-Constant C (2005) Integrin-growth factor interactions as regulators of oligodendroglial development and function. *Glia* 49(4):467–479.
54. Zhao C, Fancy SP, Franklin RJ, ffrench-Constant C (2009) Up-regulation of oligodendrocyte precursor cell alphaV integrin and its extracellular ligands during central nervous system remyelination. *J Neurosci Res* 87(15):3447–3455.
55. Whitman LM, Blanc CA, Schaumburg CS, Rowitch DH, Lane TE (2012) Olig1 function is required for remyelination potential of transplanted neural progenitor cells in a model of viral-induced demyelination. *Exp Neurol* 235(1):380–387.
56. Matheu MP, et al. (2013) Three phases of CD8 T cell response in the lung following H1N1 influenza infection and sphingosine 1 phosphate agonist therapy. *PLoS ONE* 8(3):e58033.